ACS OMEGA

http://pubs.acs.org/journal/acsodf

Article

Impact of Microporous Layer on Heat and Mass Transfer in a Single Cell of Polymer Electrolyte Fuel Cell Using a Thin Polymer Electrolyte Membrane and a Thin Gas Diffusion Layer Operated at a High-Temperature Range

Akira Nishimura,* Tatsuya Okado, Yuya Kojima, and Eric Hu

Cite This: *ACS Omega* 2021, 6, 14575−14584

Read Online

ACCESS | Metrics & More | Article Recommendations

ABSTRACT: The impact of microporous layer (MPL) on the heat- and mass-transfer characteristics and power generation performance of a polymer electrolyte fuel cell using a thin polymer electrolyte membrane (PEM) and a thin gas diffusion layer (GDL) is investigated in this paper. The power generation is investigated at the operational temperatures of 90 and 100 °C which are the target temperatures from year 2020 to 2025 according to the New Energy and Industrial Technology Development Organization's road map in Japan. The in-plane temperature distributions on the separator back at the anode and the cathode are also measured by a thermograph. As a result, it is found that the voltage drop with the MPL at a high current density is larger compared to that without the MPL irrespective of the initial temperature of the cell and relative humidity conditions. The study also revealed from the anode side observation that the in-plane temperature distribution with the MPL is wider compared to that without the MPL, especially at the initial temperature of 90 °C of the cell . Similarly, from the cathode side observation, the in-plane temperature distributions with the MPL were found to be wider compared to that without the MPL. This study has concluded that the MPL is not effective in obtaining a high performance and even an in-plane temperature distribution for a polymer electrolyte fuel cell with the thin PEM and the thin GDL at a high operational temperature range.

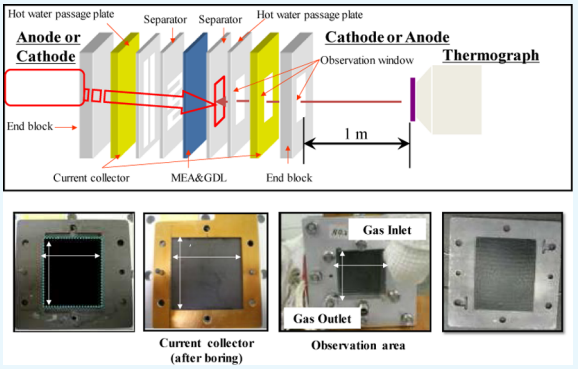

1. INTRODUCTION

Renewable H_2 is one of possible means to solve the global warming problem. A fuel cell uses renewable H_2 as the fuel. According to the New Energy and Industrial Technology Development Organization (NEDO)'s road map in Japan,[1] a polymer electrolyte fuel cell (PEFC) is required to be operated at around 90 and 100 °C for stationary application and mobility application, respectively, from year 2020 to 2025. However, the PEFC having a polymer electrolyte membrane (PEM) such as Nafion is normally operated at the temperature ranging from 60 to 80 °C.[2,3] If the PEFC is operated at a relatively higher temperature (i.e., around 90 and 100 °C), the following advantages can be expected: (i) enhancement in the electrochemical kinetics of electrodes at the anode and the cathode, (ii) size reduction of the cooling stack system because of a higher temperature difference between the stack of PEFC and the coolant, and (iii) durability enhancement toward CO and availability of lower quality reformed hydrogen.[4] However, we have to consider the following problems at the same time: (i) degradation of the membrane material, (ii) catalyst corrosion, and (iii) gas flows, pressure, temperature, and nonuniform distributions of voltage and current in the PEFC. These problems must be resolved in order to commercialize PEFC operating in a relatively high-temperature range.[5] Consequently, it is necessary to analyze heat- and mass-transfer mechanisms in the PEFC to enhance the power generation performance and stability in the high-temperature range.

The present study focuses on the analysis of in-plane temperature distribution in a single PEFC. The operating temperature has impacts on electrochemical reaction kinetics, resulting in the fact that the performance of the PEFC is also influenced by the operating temperature seriously. In addition, the PEM could be damaged by the thermal stress caused by the nonuniform temperature distribution.[6,7] Moreover, the non-

Received: March 31, 2021
Accepted: May 19, 2021
Published: May 28, 2021

https://doi.org/10.1021/acsomega.1c01693
ACS Omega 2021, 6, 14575−14584

uniform temperature distribution could also cause problems like water flooding, membrane dehydration, and cell failure due to overheating.[8] Consequently, the heat transfer in the PEFC must be controlled to achieve a uniform temperature distribution for practical realization, especially when operated in a relatively high-temperature range.

It is necessary to understand the temperature distribution first for the management of heat-transfer phenomena in the PEFC. Thermocouples are widely used for temperature measurements. However, thermocouples influence not only power generation but also accuracy in temperature measurement remarkably due to gas leak.[9,10] On the other hand, a thermograph can measure the temperature more accurately under different power generation conditions because of its nondisturbance and in situ procedure. Previous studies[7,11,12] reported that temperature distributions were measured by a thermograph below 60 °C under dry gas supply condition. There are no other studies available in the literature which revealed the temperature distribution in the PEFC at a high temperature over 80 °C, except the studies reported by the authors.[13−15]

This study takes aim at operation over 90 °C according to the NEDO road map 2017 in Japan.[1] This study selects the popular and commercial PEM and gas diffusion layer (GDL). The operational temperature of the current study is over 90 °C, which is higher compared to usual operations. Though new material membranes have been developed and reported for the high-temperature operation of PEFC,[16−18] the new material membranes have not been commercialized yet due to stability, performance, cost, and so on. If we can use the popular and commercial PEM and GDL at high temperatures, the authors think that the stationary and mobility application of the PEFC system will become popular easily. There are a few studies[19−22] investigating the effect of PEM and GDL's thicknesses on not only heat- and mass-transfer phenomena but also power generation performance of PEFC operated at a relatively higher temperature such as 90 °C. When the thinner PEM is used, lower Ohmic resistance as well as higher proton flux ratio and back diffusion can be obtained.[19,20,22] In addition, thin GDL contributes to uniform O_2 concentration distribution in the catalyst layer and water discharge performance in the PEFC.[23] Therefore, the heat- and mass-transfer phenomena as well as the power generation performance of the PEFC can be promoted by decreasing the PEM's and GDL's thicknesses. However, only a few studies[24−26] have reported the coupled effect of using both the thin PEM and the thin GDL. Additionally, microporous layer (MPL), which can improve the (i) reduction of Ohmic losses due to enhancing the hydration of PEM,[27] (ii) O_2 diffusion in the catalyst layer due to discharging water,[28] and (iii) back diffusion from the cathode to the anode by the increase in the water vaporized due to increase in the temperature of the catalyst layer at the cathode,[29] plays an important role in the PEFC. Under high-temperature operation condition, it is thought that the heat and mass transfer should be controlled strictly since it is easy to be dried up. According to previous study,[27] the addition of MPL helps to reduce Ohmic loss due to enhancement of hydration of PEM. In addition, the MPL can reduce liquid water flooding in the GDL, resulting in enhanced transport of gaseous species and minimized mass transport limitations. However, these effects of MPL are discussed under normal operation temperature condition. Since it can be thought that the content of liquid water is small under high-temperature operation condition, the function of MPL, which is enhancement of water transfer, might not be conducted well. Therefore, this study thinks it is necessary to verify whether these effects of MPL are obtained or not under high-temperature operation condition. However, there are no reports on the effect of MPL on heat- and mass-transfer characteristics and power generation performance of PEFC with the thin PEM and thin GDL operated at a high temperature such as 90 °C.

This study aims to analyze the impact of MPL on the heat- and mass-transfer characteristics and power generation performance of the PEFC with the thin PEM and the thin GDL operated at a relatively high temperature (e.g., 90 and 100 °C). This study measured in-plane temperature distributions on the anode and cathode separator back using a thermograph by changing the operation temperature, relative humidity (RH), and flow rate of inflow gases. The voltage and local current to evaluate the performance of the PEFC have also been measured and analyzed.

2. RESULTS AND DISCUSSION

2.1. Impact of MPL on Power Generation Performance. Figures 1 and 2 show the polarization curves without and with MPL at the initial temperature of the cell (T_{ini}) = 90 °C under various RH conditions, respectively. Figures 3 and 4 show the polarization curves without and with MPL at T_{ini} = 100 °C under various RH conditions, respectively.

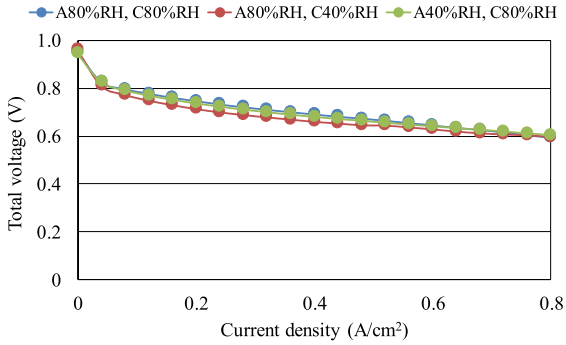

Figure 1. Polarization curves without MPL among different RH conditions at T_{ini} = 90 °C.

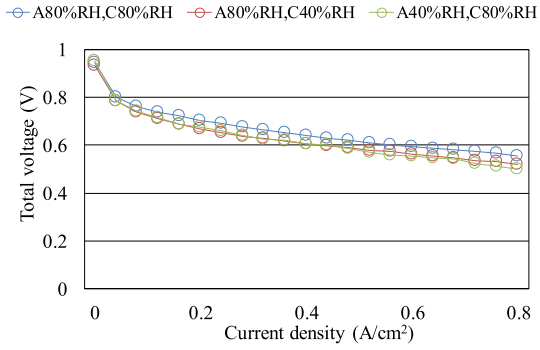

Figure 2. Polarization curves with MPL among different humidity conditions at T_{ini} = 90 °C.

According to these figures, it is found that the voltage drop with the MPL at a high current density is larger compared to that without MPL irrespective of T_{ini} and RH conditions. As the water production rate increased with the increased current

https://doi.org/10.1021/acsomega.1c01693
ACS Omega 2021, 6, 14575−14584

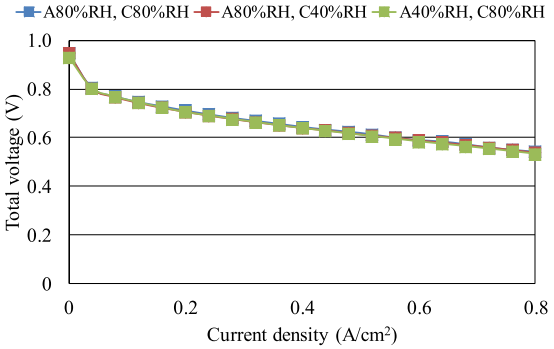

Figure 3. Polarization curves without MPL among different RH conditions at T_{ini} = 100 °C.

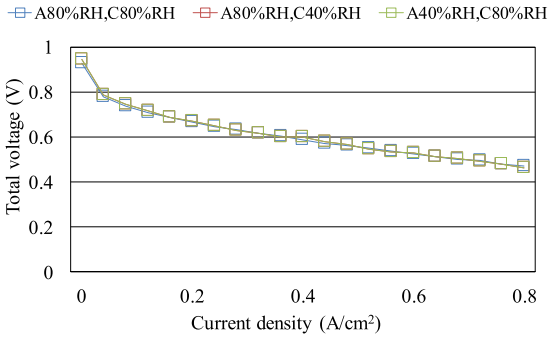

Figure 4. Polarization curves with MPL among different RH conditions at T_{ini} = 100 °C.

density, the condensation of water in the pores of GDL would occur easily,[30] which would cause the flooding. The MPL could assist to prevent flooding by discharging the liquid water from the catalyst layer to the GDL at a medium temperature such as 60 °C.[30] However, it was observed that the voltage decreased at a high current density with MPL more than that without MPL in this study. However, the operation temperatures of T_{ini} = 90 and 100 °C in this study were easy to dry up PEM, resulting in the negative effect of the function of MPL, which promotes to discharge the liquid water from the catalyst layer. Consequently, it was observed that the voltage drop with MPL at a high current density was more than that without MPL.

Therefore, it was believed that the removal of water from the catalyst layer to the separator occurred smoothly in this study because of the thin GDL used. Although in this study, the influence of RH conditions on the power generation performance has been investigated, it has not been confirmed distinctively. Using a thin PEM and a thin GDL could enhance water transfer between both electrodes, especially under low RH conditions at one side. As a result, it is thought that the power generation performance under low RH conditions at one side could reach the same level as that under well-humidified conditions such as the anode with 80% RH and cathode with 80% RH (A80%RH, C80%RH).

2.2. Impact of MPL on In-Plane Temperature Distribution. Figures 5−8 show the in-plane temperature distributions at the anode side without and with MPL at T_{ini} = 90 and 100 °C with changing RH of the inflow gas, respectively. Since the impact of stoichiometric ratio of the inflow gas on the in-plane temperature distribution was not conformed, the results obtained for the stoichiometric ratio of 1.5 are shown here. In addition, the standard deviation for in-plane temperature distributions for each condition is also shown in Table 1.

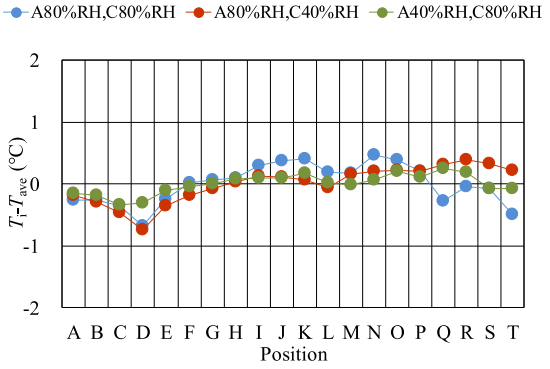

Figure 5. Comparison of in-plane temperature distribution on the anode side without MPL at T_{ini} = 90 °C among different RH conditions.

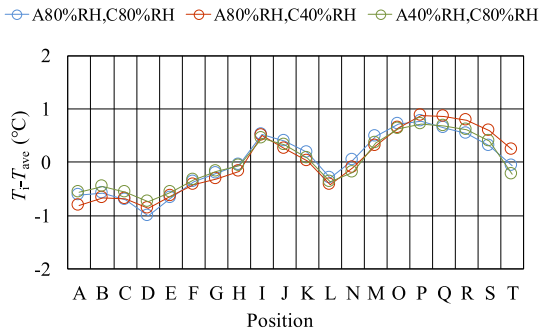

Figure 6. Comparison of in-plane temperature distributions on the anode side with MPL at T_{ini} = 90 °C among different RH conditions.

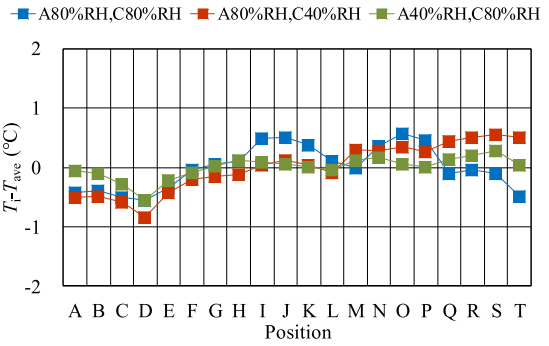

Figure 7. Comparison of in-plane temperature distributions on the anode side without MPL at T_{ini} = 100 °C among different RH conditions.

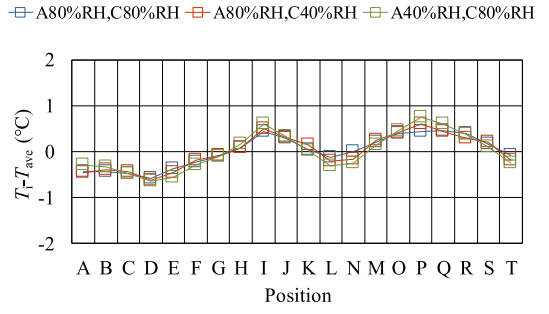

Figure 8. Comparison of in-plane temperature distributions on the anode side with MPL at T_{ini} = 100 °C among different RH conditions.

https://doi.org/10.1021/acsomega.1c01693
ACS Omega 2021, 6, 14575−14584

Table 1. Comparison of Standard Deviation of In-Plane Temperature Distributions on the Anode Side for Each Condition

T_{ini} = 90 °C								T_{ini} = 100 °C							
MPL W/O			MPL W			MPL W/O			MPL W						
A80%RH, C80%RH	A80%RH, C40%RH	A40%RH, C80%RH	A80%RH, C80%RH	A80%RH, C40%RH	A40%RH, C80%RH	A80%RH, C80%RH	A80%RH, C40%RH	A40%RH, C80%RH	A80%RH, C80%RH	A80%RH, C40%RH	A40%RH, C80%RH	A80%RH, C80%RH	A80%RH, C40%RH	A40%RH, C80%RH	A80%RH, C80%RH
0.32	0.29	0.16	0.54	0.59	0.48	0.37	0.41	0.19	0.34	0.37	0.41				

According to these figures, it is observed that the difference of in-plane temperature distributions in the latter half of the observation area among various RH conditions without MPL is larger compared to that with MPL irrespective of T_{ini}. In other words, the temperature for anode 80% RH and cathode 80% RH without MPL decreases larger near the outlet compared to the other RH conditions without MPL. The gas diffusion inhibition by liquid water accumulation was smaller under high-temperature condition such as T_{ini} = 90 and 100 °C, resulting in the fact that PEM might have been hydrated with the water in gas flow through the gas channel.[13] As a result, the temperature increases along the gas channel.[13] It can be seen from Figures 5 and 7 that the temperature generally increases toward the outlet although the temperature at some positions decreases. However, as mentioned above, the temperature for anode 80% RH and cathode 80% RH without MPL decreases more near the outlet compared to other RH conditions without MPL. Since anode 80% RH and cathode 80% RH is a well-humidified condition, it is believed that the water generated at the cathode is more compared to that under the other RH conditions. Since this study uses a thin PEM, the back diffusion from the cathode to anode occurs easily.[19,20,22] Therefore, the gas diffusion inhibition by water accumulation would occur near the outlet of the cell at the anode side for anode 80% RH and cathode 80% RH without MPL, resulting in the decrease of temperature. As to the temperature drop near position D which was observed under every condition, position D was on the opposite side through the cell, which has been located at the inlet of gas flow, and the temperature of the supply gas was colder than the cell temperature, resulting in a temperature drop.[13,31]

Additionally, it is found from Figures 5−8 that the in-plane temperature distributions with MPL are wider compared to those without MPL. In addition, it can also be observed from the comparison of standard deviations shown in Table 1, especially at T_{ini} = 90 °C. Strictly speaking, the temperature drops at position L and at the positions near the outlet were larger in the case with MPL. Position L is located at the corner of the serpentine channel. MPL promotes the back diffusion from the cathode to the anode by the increase in the water vaporized due to increase in the temperature of the catalyst layer at the cathode.[29] In addition, thin PEM also promotes the back diffusion from the cathode to the anode.[19,20,22] As a result, it is believed that the water content in the anode increases. Since position L is located at the corner of the serpentine channel, the water might stick there.[32,33] Additionally, it is thought that the water flowing along the channel with the gas accumulates near the outlet.[31] Therefore, the gas diffusion inhibition is caused at position L as well at as the positions near the outlet, resulting in the temperature drop. Although the water might be accumulated along the flow direction, the temperature drops at position L and then increases again as shown in Figures 5 and 7. According to previous study[34] with the experimental observation of water behavior in the GDL and gas channel, the cross-flow in GDL might have occurred under the land area, which promotes the power generation around the area where the liquid water is accumulated. This might be the reason that the temperature increases again after position L.

Figures 9−12 show the in-plane temperature distributions on the cathode side without and with MPL at T_{ini} = 90 and 100 °C, changing the RH of inflow gas, respectively. Since the impact of stoichiometric ratio of the inflow gas on the in-plane

https://doi.org/10.1021/acsomega.1c01693
ACS Omega 2021, 6, 14575−14584

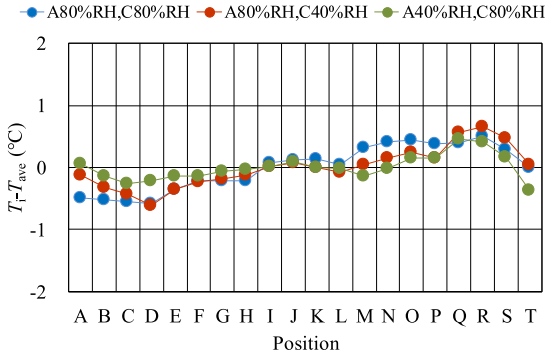

Figure 9. Comparison of in-plane temperature distributions on the cathode side without MPL at T_{ini} = 90 °C among different RH conditions.

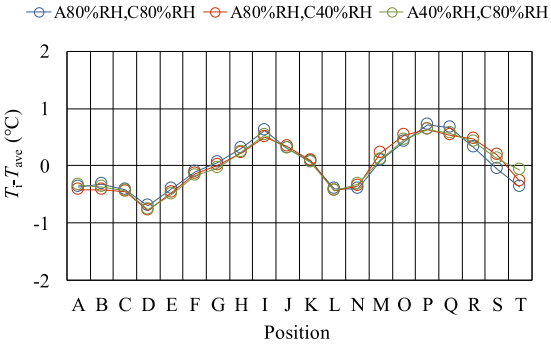

Figure 10. Comparison of in-plane temperature distributions on the cathode side with MPL at T_{ini} = 90 °C among different RH conditions.

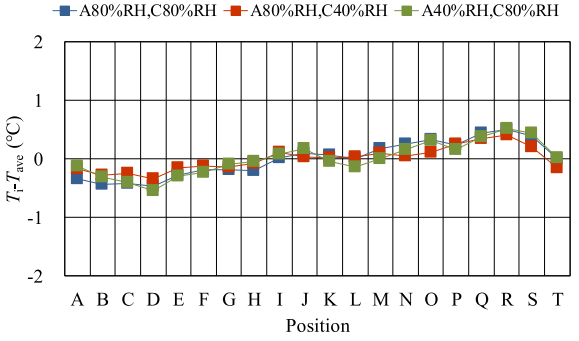

Figure 11. Comparison of in-plane temperature distributions on the cathode side without MPL at T_{ini} = 100 °C among different RH conditions.

temperature distribution was not confirmed, the results obtained for the stoichiometric ratio of 1.5 are shown here. In addition, the standard deviation for in-plane temperature distributions for each condition is also shown in Table 2.

It can be seen from Figures 9 and 11 that the temperatures increase through the gas channel generally, although they drop near the outlet in the case without MPL. The gas diffusion inhibition by liquid water accumulation was smaller under high-temperature condition such as T_{ini} = 90 and 100 °C, resulting in the fact that the PEM might have been hydrated with the water in the gas flow through the gas channel.[13] It causes the increase in temperature through the gas channel.[13] According to the authors' previous study,[13] the in-plane temperature distribution at the cathode is wider than that at the anode since the temperature at the corner drops by the gas

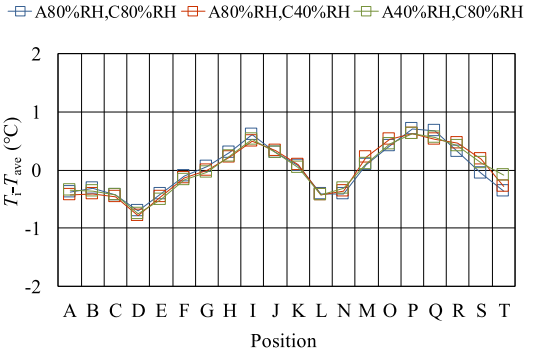

Figure 12. Comparison of in-plane temperature distributions on the cathode side with MPL at T_{ini} = 100 °C among different RH conditions.

diffusion inhibition due to water produced by the electrochemical reaction as well as humidification water in the gas for supply to the cell existed at the cathode. However, in this study, the in-plane temperature distributions at the cathode without MPL were not wider as shown in Figures 9 and 11. Since this study uses a thin PEM, the back diffusion from the cathode to the anode might occur easily.[19,20,22] Therefore, it is believed that the gas diffusion inhibition due to water accumulation at the corner might not occur except at the position near the outlet. As to the position near the outlet, it is believed that the water may accumulate near the outlet[31] even though the back diffusion occurs.

On the other hand, it is observed that the in-plane temperature distributions with MPL are wider compared to that without MPL according to Figures 9−12. In addition, it can be observed from the comparison of standard deviations shown in Table 2, especially at T_{ini} = 90 °C. It is obvious that the temperatures drop at position L as well as at positions near the outlet in the case with MPL. Since this study uses a thin PEM and a thin GDL, lower Ohmic resistance, higher proton flux ratio of PEM,[19,20,22] and reduction in mass transfer loss in GDL[23] were obtained. Therefore, the power generation performance is promoted, resulting in an increase in the water produced by O_2 reduction reaction in the cathode. MPL might support water transfer from the catalyst layer to the GDL by capillary pressure at the cathode,[35] and the water was discharged into the separator. As a result, the gas in the channel flows with the accumulation of water. As described above, water is easy to remain at the corner of the serpentine channel,[32,33] resulting in the decrease in the temperature of the separator back due to gas diffusion inhibition.

It has been concluded in the previous section that MPL is not effective in improving the performance and even in-plane temperature distribution when using a thin PEM and a thin GDL at a high temperature. According to previous study by the authors,[35] MPL has been effective in improving the power generation performance when using a thick PEM and a thick GDL whose thicknesses are 127 and 190 μm, respectively, while the in-plane temperature distribution was not even. According to previous studies,[29,36,37] the thermal conductivity, thickness, porosity, and wettability of the MPL influence the mass and heat transfer in the catalyst layer and GDL. The MPL consists of a powdery mixture of carbon black and polytetrafluoroethylene (PTFE) particles, which is sprayed onto the GDL and then sintered, so the PTFE can bind the powder together.[27] It is believed that the thermal conductivity

https://doi.org/10.1021/acsomega.1c01693
ACS Omega 2021, 6, 14575−14584

Table 2. Comparison of Standard Deviation of In-Plane Temperature Distributions on the Cathode Side for Each Condition

T_{ini} = 90 °C								T_{ini} = 100 °C							
MPL W/O				MPL W				MPL W/O				MPL W			
A80%RH, C80%RH	A80%RH, C40%RH	A40%RH, C80%RH	A80%RH, C80%RH	A80%RH, C40%RH	A40%RH, C80%RH			A80%RH, C80%RH	A80%RH, C40%RH	A40%RH, C80%RH	A80%RH, C80%RH	A80%RH, C40%RH	A40%RH, C80%RH		
0.37	0.32	0.20	0.42	0.43	0.41			0.31	0.21	0.28	0.42	0.43	0.41		

and wettability of MPL are influenced by the mixture ratio of carbon black and PTFE particles. It is also important to consider the type of GDL such as carbon paper or carbon cloth in order to obtain the effect of MPL.[27] In this study, only one type of MPL as well as GDL was investigated. Under the high operation temperature condition, it is necessary to optimize the water content in the PEM and catalyst layer, which influences the power generation performance as well as the temperature distribution, since it is easy to be dried up. This study thinks the reason why the even in-plane temperature distribution with MPL was not obtained is that the combination of MPL, PEM, catalyst layer, and GDL was not optimized. Therefore, this study suggests to investigate their combination by changing the physical properties and structure, for example, thermal conductivity, thickness, porosity, and wettability of MPL, in order to obtain high power generation performance as well as in-plane temperature distribution at the same time in the near future.

3. CONCLUSIONS

This study investigated the impact of MPL on the heat- and mass-transfer characteristics and power generation performance of PEFC with a thin PEM and a thin GDL operating at a relatively high temperature. This study measured the in-plane temperature distributions on the anode and cathode separator back using a thermograph as well as the voltage and local current to evaluate the performance of PEFC. The following conclusions are drawn from the study

(1) The voltage drop with MPL at a high current density was larger compared to that without MPL irrespective of T_{ini} and RH conditions. Since T_{ini} = 90 and 100 °C are easy to dry up PEM, the function of MPL promoting to discharge the liquid water from the catalyst layer actually resulted in a negative effect.
(2) At the anode side, the temperature for anode 80% RH and cathode 80% RH without MPL decreases larger near the outlet compared to the other RH conditions without MPL. In addition, the in-plane temperature distribution with MPL was more compared to that without MPL irrespective of T_{ini}.
(3) At the cathode side, the temperature increases through the gas channel generally, although dropping near the outlet in the case without MPL. In addition, the in-plane temperature distribution with MPL is wider compared to that without MPL.
(4) MPL is not effective in improving the performance and even in-plane temperature distribution when used with a thin PEM and a thin GDL at a high temperature.

4. EXPERIMENTAL PEFC SYSTEM

4.1. Experimental Setup and Procedure. In this study, a single cell PEFC (MC-25-SC-NH; manufactured by Reactive Innovations) and Nafion NRE-211 (manufactured by DuPont Corp.) with a thickness of 25 μm and TGP-H-030 (manufactured by Toray Corp.) with a thickness of 110 μm were used as PEM and GDL, respectively. Table 3 lists the specifications of the cell components used in this study. Figure 13 illustrates the experimental procedure of temperature measurements. Figure 13 also shows the cell structures to measure the temperature.[38−40] The hole for temperature measurement observations had a size of 50 mm × 50 mm, which was the same size as the electrode. The hot water

https://doi.org/10.1021/acsomega.1c01693
ACS Omega 2021, 6, 14575−14584

Table 3. Specifications of PEFC Components

components	dimension	information
PEM	width is 50.0 mm, height is 50.0 mm, thickness is 0.025 mm	Nafion NRE-211 (manufactured by DuPont Corp.)
catalyst layer	width is 50.0 mm, height is 50.0 mm (fitted on PEM)	Pt loaded on carbon (loading ratio of Pt is 20 wt %)
GDL	width is 50.0 mm, height is 50.0 mm, thickness is 0.110 mm	TGP-H-030 (manufactured by Toray Corp.)
gas separator	width is 75.4 mm, height is 75.4 mm, thickness is 2.00 mm (the area whose width is 50.0 mm and height is 50.0 mm is for gas supply)	made by carbon graphite, serpentine flow
hot water passage plate	width is 75.4 mm, height is 75.4 mm, thickness is 2.00 mm	made by carbon graphite
current collector	power generation area is 6937 mm^2, thickness is 2.00 mm	made by copper coated with gold
end block	width is 110 mm, height is 110 mm, thickness is 12.7 mm	made by alumina

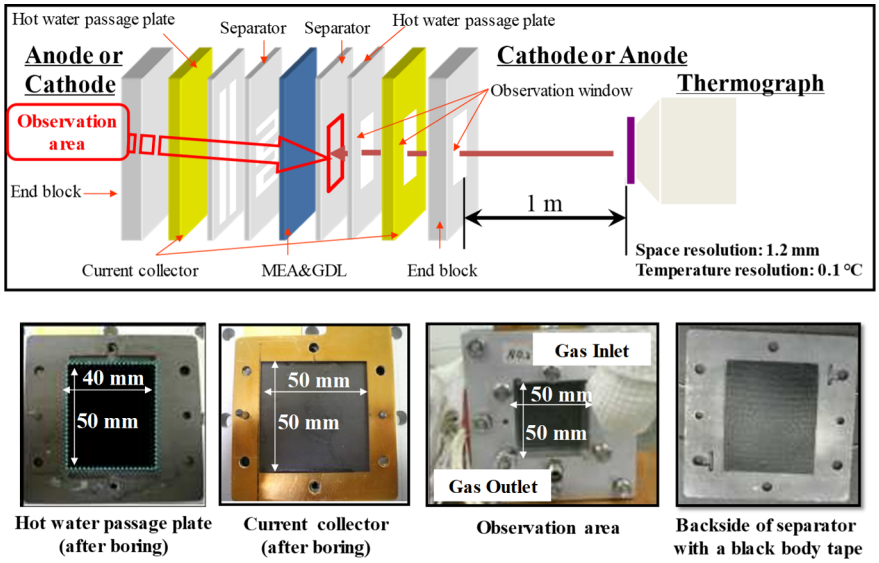

Figure 13. PEFC structure for temperature measurement through a thermograph (photos are taken by authors).

passage plate had a hole whose dimension was 40 mm × 50 mm.

We measured the in-plane temperature distributions on the anode and cathode separator back through the hole using a thermograph (Thermotracer TH9100WL; manufactured by NIPPON AVONICS Co., Ltd.). In Figure 13, the space resolution and temperature resolution of the thermograph are also given. The space resolution means the length guaranteeing the accuracy of the measured temperature. The temperature resolution means the temperature difference guaranteeing the accuracy of the measured temperature. In addition, the temperature data is analyzed using the dedicated software (TH91-702; manufactured by NIPPON AVIONICS Co., Ltd.). A black body tape (HB-250; manufactured by OPTIX) with a thickness of 0.1 mm on the separator back was fitted to prevent the measurement inaccuracy caused by the surface roughness and reflection variation. It is necessary to understand the emissivity of the black body tape used for the power generation experiment. Therefore, it was measured before the experiment. In addition, it has been confirmed before the experiment that the impact of the observation window on the power generation performance was very little. The initial temperature of the single cell was 70 °C, and the RHs of both inflow gases were 80% RH with and without a hole for observations.[38,39] According to the results obtained in the pre-experiment, it has been confirmed that the voltage drops due to observation window at the current (load) density of 0.80 A/cm^2 during the anode and cathode observation experiments have been only 4 and 7%, respectively. Consequently, the impact of the observation window on the power generation performance was ignored in this study.

In this study, all sides of the cell excluding the observation window side and opposite side were thermally insulated. The in-plane temperature distribution caused by the reaction heat was measured by a thermograph. The current density of 0.80 A/cm^2 was kept, so the temperature of single cell could be maintained without any heat input from the electric heater.[38,39] The thermal conductivities of PEM, GDL, and separator are 0.195, 1.7, and 25 W/(m K), respectively, according to the manufacturer's descriptions. The thermal conductivities of the hot water passage plate, current collector, and end block are 25, 380, and 220 W/(m K), respectively. Since the thermal conductivities of the hot water passage plate, current collector, and end block located outside of the separator are higher than those of the PEM, GDL, and separator, there is no impact of ambient air on the temperature distribution.[38,39] It was found that the gas leak occurred if no hot water passage plate was assembled in advance. Therefore, the hot water passage plate was installed to prevent the gas leak without flowing hot water.

Table 4 lists the experimental operating conditions and parameters. Figure 14 illustrates the experimental setup. The temperature of inflow gases was controlled in order to maintain the same temperature as T_{ini}. The RH of inflow gases was controlled by humidifiers and dew point meters (MHT337FC;

https://doi.org/10.1021/acsomega.1c01693
ACS Omega 2021, 6, 14575−14584

Table 4. Experimental Operation Conditions

initial temperature (T_{ini}) (°C)	90, 100	
load current (A) [current density (A/cm^2)]	0–20 (0–0.80)	
Inflow Gas Condition		
	anode	cathode
gas characteristics	H_2 whose purity is 99.995 vol %	O_2 whose purity is 99.995 vol %
temperature of inflow gas (°C)	90, 100	90, 100
RH of inflow gas (% RH)	40, 80	40, 80
pressure of inflow gas (absolute) (MPa)	0.4	0.4
flow rate of inflow gas (NL/min) [stoichiometric ratio (−)]	0.210, 0.280, 0.420 (1.5, 2.0, 3.0)	0.105, 0.140, 0.210 (1.5, 2.0, 3.0)

manufactured by VAISALA). This study kept the flow rates of inflow gases at the stoichiometric ratios of 1.5, 2.0, and 3.0 and used pure H_2 and pure O_2 at the anode and the cathode as the fuel and the oxidant. This study controlled the flow rate of inflow gases using the mass flow controller (5850E; manufactured by BROOKS INSTRUMENT). In this study, the flow rate of inflow gas with a stoichiometric ratio of 1.0 is defined by eq 1.

$$C_{H_2} = I/nF \tag{1}$$

where C_{H_2} is the molar flow rate of H_2 (mol/s), I is the load current (A), n is the valence ion (=2) (−), and F is Faraday constant (=96,500) (C/mol). C_{H_2} is the same as the amount of H_2 whose stoichiometric ratio is 1.0. C_{O2} indicates the molar flow rate of O_2 (mol/s) which is equal to a half of C_{H2} (can be understood from eq 2).

$$H_2 + 1/2O_2 = H_2O \tag{2}$$

The load current of PEFC was controlled by the electric device (PLZ603W; manufactured by KIKUSUI ELECTRONICS CORP.). The total voltage according to the load current was also controlled by the electric load device.

In this experiment, the cell was heated for startup using electric heaters (Silicon rubber heater MG; manufactured by OM Heater) which were installed around the end block. We heated H_2 and O_2 at T_{ini} before suppling into the cell at the startup process. After attaining T_{ini}, the PEFC power generation was carried out by changing the load. The flow rates of inflow gases and temperature distribution were maintained as steady state for over 30 min by keeping the load current unchanged.

4.2. Method of Temperature Image/Thermograph Evaluation. The temperature images are obtained using the thermograph by dividing into segments. As shown in Figure 15, the image of in-plane temperature distribution was divided

Figure 15. Segment of the temperature range.

into the area having a vertical length of 10 mm and a horizontal length of 10 mm. The number of areas are 20 indexed from A to T following the direction of the gas flow along the gas channel. The mean temperature in each area was calculated using the temperature image. The temperatures of areas A and T were measured by removing the area where the thermal insulator covering the gas pipe disturbed to detect the infrared ray by the thermograph.

The temperature difference $T_i - T_{ave}$ (°C) is used as the criterion to indicate in-plane temperature distribution, where T_i indicates the average temperature in respective areas (A to T) and T_{ave} indicates the mean temperature among all areas. T_{ave} is defined by the following equation

$$T_{ave} = \frac{\sum_{i=A}^{T} T_i}{20} \tag{3}$$

4.3. Analytical Method. This study uses dedicated software to analyze the temperature distribution measured by the thermograph. The minimum resolution of temperature and space measured by the thermograph is 0.1 °C and 1 mm, respectively. The mean temperature in each area, which was divided into 20 from the whole temperature image, was calculated using the temperature image having 29 × 29 digital data. As to areas A and T, the digital data of the area disrupted by the thermal insulator covering the gas pipe were removed for the calculation of the mean temperature as mentioned above. This study adopts the temperature difference $T_i - T_{ave}$ to evaluate the gradient of in-plane temperature distribution.

AUTHOR INFORMATION

Corresponding Author

Akira Nishimura − *Division of Mechanical Engineering, Graduate School of Engineering, Mie University, 514-8507*

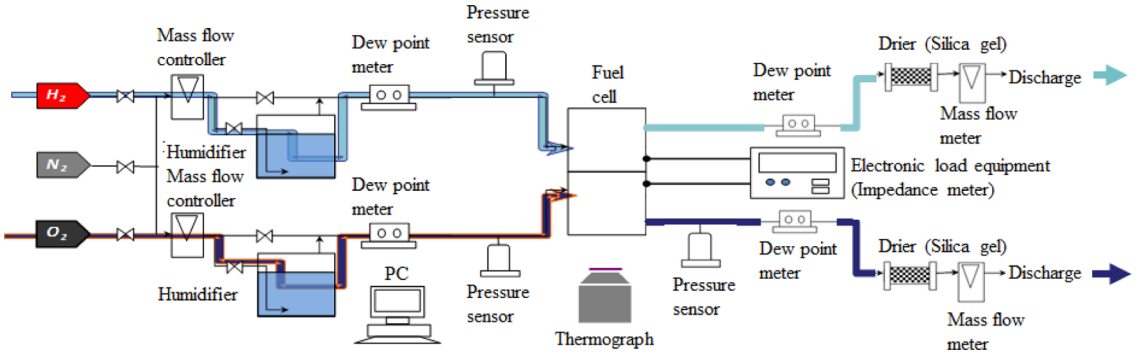

Figure 14. Schematic diagram of the experimental setup.

https://doi.org/10.1021/acsomega.1c01693
ACS Omega 2021, 6, 14575−14584

Tsu, Japan; orcid.org/0000-0002-4120-5112;
Email: nisimura@mach.mie-u.ac.jp

Authors

Tatsuya Okado − *Division of Mechanical Engineering, Graduate School of Engineering, Mie University, 514-8507 Tsu, Japan*

Yuya Kojima − *Division of Mechanical Engineering, Graduate School of Engineering, Mie University, 514-8507 Tsu, Japan*

Eric Hu − *School of Mechanical Engineering, The University of Adelaide, Adelaide 5005, South Australia, Australia*

Complete contact information is available at:
https://pubs.acs.org/10.1021/acsomega.1c01693

Notes

The authors declare no competing financial interest.

■ ACKNOWLEDGMENTS

This study was supported by the Mie Industrial Research Institute.

■ ABBREVIATIONS

C_{H_2}, molar flow rate of H_2 (mol/s)
C_{O_2}, molar flow rate of O_2 (mol/s)
F, Faraday constant (=96,500) (C/mol)
I, load current (A)
n, valence ion (=2) (−)
T_{ave}, mean temperature among all areas (°C)
T_i, average temperature in respective area (°C)
T_{ini}, initial temperature of cell (°C)

■ REFERENCES

(1) New Energy and Industrial Technology Development Organization (NEDO). http://www.nedo.go.jp/news/press/AA5_100889.html. 2018, (accessed Dec 4, 2018).
(2) Zhang, G.; Kandlikar, S. G. A Critical Review of Cooling Technique in Proton Exchange Membrane Fuel Cell Stacks. *Int. J. Hydrogen Energy* **2012**, *37*, 2412−2429.
(3) Agbossou, K.; Kolhe, M.; Hamelin, J.; Bose, T. K. Performance of a Stand-alone Renewable Energy System Based on Energy Storage at Hydrogen. *IEEE Trans. Power Appar. Syst.* **2004**, *19*, 633−640.
(4) Li, Q.; He, R.; Jensen, J. O.; Bjerrum, N. J. Approaches and Recent Development Polymer Electrolyte Membrane for Fuel Cells Operating above 100 °C. *Chem. Mater.* **2003**, *15*, 4896−4915.
(5) Lee, C.-Y.; Weng, F.-B.; Kuo, Y.-W.; Tsai, C.-H.; Cheng, Y.-T.; Cheng, C.-K.; Lin, J.-T. In-situ Measurement of High-temperature Proton Exchange Membrane Fuel Cell Stack Using Flexible Five-in-one Micro Sensor. *Sensors* **2016**, *16*(), doi: DOI: 10.3390/s16101731.
(6) Tsuji, K. Domestic Fuel Cell Co-generation System Entering Real Commercial Stage. *Hydrogen Energy Syst.* **2008**, *33*, 93−96.
(7) Wang, M.; Guo, H.; Ma, C. Temperature Distribution on the MEA Surface of a PEMFC with Serpentine Channel Flow Bed. *J. Power Sources* **2006**, *157*, 181−187.
(8) Zhang, G.; Guo, L.; Ma, L.; Liu, H. Simultaneous Measurement of Current and Temperature Distributions in a Proton Exchange Membrane Fuel Cell. *J. Power Sources* **2010**, *195*, 3597−3604.
(9) Ogawa, T.; Hohara, N.; Chikahisa, T.; Hishimura, Y. Observation of Water Production and Temperature Distribution in PEM Fuel Cell. *Proceedings of the 41st National Heat Transfer Symposium of Japan;*Heat Transfer Society of Japan, 2004; pp 235−236.
(10) Ogawa, T.; Chikahisa, T.; Kikuta, K. Measurement of Fluctuating Distribution in PEFC due to Produced Water. *Proceedings of Thermal Engineering Conference*, 2003; pp 483−484.
(11) Hakenjos, A.; Muenter, H.; Wittstadt, U.; Hebling, C. A PEM Fuel Cell for Combined Measurement of Current and Temperature Distribution, and Flow Field Flooding. *J. Power Sources* **2004**, *131*, 213−216.
(12) Ogawa, T.; Hohan, N.; Chikahisa, T.; Hishimura, Y. Prospect of Water Production and Temperature Distribution in PEM Fuel Cell. *Therm. Sci. Eng.* **2004**, *23*, 93−94.
(13) Nishimura, A.; Yoshimura, M.; Mahadi, A. H.; Hirota, M.; Kolhe, M. L. Impact of Operation Condition on Temperature Distribution in Single Cell of Polymer Electrolyte Fuel Cell Operated at Higher Temperature than Usual. *Mech. Eng. J.* **2016**, *3*, 16-00304.
(14) Nishimura, A.; Yoshimura, M.; Kamiya, S.; Hirota, M.; Eric, H. Impact of Relative Humidity of Supply Gas on Temperature Distributions in Single Cell of Polymer Electrolyte Fuel Cell when Operated at High Temperature. *J. Energy Power Eng.* **2017**, *11*, 706−718.
(15) Nishimura, A.; Kamiya, S.; Okado, T.; Sato, Y.; Hirota, M.; Kolhe, M. L. Heat and Mass Transfer Analysis in Single Cell of PEFC Using Different PEM and GDL at Higher Temperature. *Int. J. Hydrogen Energy* **2019**, *44*, 29631−29640.
(16) Budak, Y.; Devrim, Y. Micro-cogeneration Application of a High-temperature PEM Fuel Cell Stack Operated with Polybenzimidazole Based Membranes. *Int. J. Hydrogen Energy* **2020**, *45*, 35198−35207.
(17) Kim, D.-H.; Min, C.-M.; Lee, E.; Lee, J.-S.; Pak, C. Effect of Vinylphosphonic Acid and Polymer Binders with Phosphate Groups on Performance of High-temperature Polymer Electrolyte Membrane Fuel Cell. *Catal. Today* **2020**, *358*, 333−337.
(18) Wang, D.; Wang, S.; Tian, X.; Li, J.; Liu, F.; Wang, X.; Chen, H.; Mao, T.; Liu, G. Ethly Phosphoric Acid Grafted Amiono-modified Polybenzimidazole with Improved Long-term Stability for High-temperature Proton Exchange Membrane Applications. *Int. J. Hydrogen Energy* **2020**, *45*, 3176−3185.
(19) Springer, T. E.; Zawodzinski, T. A.; Gottesfeld, S. Polymer Electrolyte Fuel Cell Models. *J. Electrochem. Soc.* **1991**, *138*, 2334−2342.
(20) Penga, Ž.; Tolj, I.; Barbir, F. Computational Fluid Dynamics Study of PEM Fuel Cell Performance for Isothermal and Non-uniform Temperature Boundary Conditions. *Int. J. Hydrogen Energy* **2016**, *41*, 17585−17594.
(21) Yablecki, J.; Bazylak, A. Determining the Effective Thermal Conductivity of Composed PEMFC GDLs through Thermal Resistance Modeling. *J. Power Sources* **2012**, *217*, 470−478.
(22) Zhu, G.; Chen, W.; Lu, S.; Chen, X. Parameter Study of High-temperature Proton Exchange Membrane Fuel Cell Using Data-driven Models. *Int. J. Hydrogen Energy* **2019**, *44*, 28958−28967.
(23) Epting, W. K.; Litster, S. Microscale Measurements of Oxygen Concentration across the Thickness of Diffusion Media in Operating Polymer Electrolyte Fuel Cells. *J. Power Sources* **2016**, *306*, 674−684.
(24) Rosli, R. E.; Sulong, A. B.; Daud, W. R. W.; Zulkifley, M. A.; Husaini, T.; Rosli, M. I.; Majlan, E. H.; Haque, M. A. A Review of High-temperature Proton Exchange Membrane Fuel Cell (HT-PEMFC) System. *Int. J. Hydrogen Energy* **2017**, *42*, 9293−9314.
(25) Quartarone, E.; Angioni, S.; Mustarelli, P. Polymer and Composite Membranes for Proton-Conducting, High-temperature Fuel Cells: a Critical Review. *Materials* **2017**, *10*,doi: DOI: 10.3390/ma10070687.
(26) Özdemir, Y.; Özkan, N.; Devrim, Y. Fabrication and Characterization of Cross-linked Polybenzimidazole Based Membranes for High Temperature PEM fuel cells. *Electrochim. Acta* **2017**, *245*, 1−13.
(27) Zamel, N.; Becker, J.; Wiegmann, A. Estimating the Thermal Conductivity and Diffusion Coefficient of the Microporous Layer of Polymer Electrolyte Membrane Fuel Cells. *J. Power Sources* **2012**, *207*, 70−80.
(28) Blanco, M.; Wilkinson, D. P. Investigation of the Effect of Microporous Layers on Water Management in a Proton Exchange Membrane Fuel Cell Using Novel Diagnostic Methods. *Int. J. Hydrogen Energy* **2014**, *39*, 16390−16404.

(29) Zhou, J.; Shukla, S.; Putz, A.; Secanell, M. Analysis of the Role of the Microporous Layer in Improving Polymer Electrolyte Fuel Cell Performance. *Electrochim. Acta* **2018**, *268*, 366−382.
(30) Quan, P.; Zhou, B.; Sobiesiak, A.; Liu, Z. Water Behaviour in Serpentine Micro-channel for Proton Exchange Membrane Fuel Cell Cathode. *J. Power Sources* **2005**, *152*, 131−145.
(31) Nishimura, A.; Yoshimura, M.; Kamiya, S.; Hirota, M.; Hu, E. Impact of Relatively Humidity of Supply Gas on Temperature Distributions in Single cell of Polymer Electrolyte Fuel Cell when Operated at High Temperature. *J. Energy Power Eng.* **2017**, *11*, 706−718.
(32) Quan, P.; Lai, M.-C. Numerical Study of Water Management in the Air Flow Channel of a PEM Fuel Cell Cathode. *J. Power Sources* **2007**, *164*, 222−237.
(33) Jiao, K.; Park, J.; Li, X. Experimental Investigations on Liquid Water Removal from the Gas Diffusion Layer by Reactant Flow in PEM Fuel Cell. *Appl. Energy* **2010**, *87*, 2770−2777.
(34) Mariani, M.; Latorrata, S.; Patrignani, S.; Gallo Stampino, P.; Dotelli, G. Characterization of Novel Graphene-based Microporous Layers for Polymer Electrolyte Membrane Fuel Cells Operating under Low humidity and High Temperature. *Int. J. Hydrogen Energy* **2020**, *45*, 7046−7058.
(35) Nishimura, A.; Okado, T.; Kojima, Y.; Hirota, M.; Hu, E. Impact of MPL on Temperature Distribution in Single Polymer Electrolyte Fuel Cell with Various Thicknesses of Polymer Electrolyte Membrane. *Energies* **2020**, *13*, 2499.
(36) Tanuma, T.; Kawamoto, M.; Kinoshita, S. Effect of Properties of Hydrophilic Microporous Layer (MPL) on PEFC Performance. *J. Electrochem. Soc.* **2017**, *164*, F499−F503.
(37) Kang, K.; Ju, H. Numerical Modeling and Analysis of Micro-porous Layer Effects in Polymer Electrolyte Fuel Cells. *J. Power Sources* **2009**, *194*, 763−773.
(38) Chen, G.; Zhang, G.; Guo, L.; Liu, H. Systematic Study on the Functions and Mechanisms of Micro Porous Layer on Water Transport in Proton Exchange Membrane Fuel Cells. *Int. J. Hydrogen Energy* **2016**, *41*, 5063−5073.
(39) Nishimura, A.; Yoshimura, M.; Mahadi, A. H.; Hirota, M.; Kolhe, M. L. Impact of Operation Condition on Temperature Distribution in Single Cell of Polymer Electrolyte Fuel Cell Operated at Higher Temperature than Usual. *Mech. Eng. J.* **2016**, *3*, 16-00304.
(40) Nishimura, A.; Kamiya, S.; Okado, T.; Sato, Y.; Hirota, M.; Kolhe, M. L. Heat and Mass Transfer Analysis in Single Cell of PEFC Using Different PEM and GDL at Higher Temperature. *Int. J. Hydrogen Energy* **2019**, *44*, 29631−29640.

https://doi.org/10.1021/acsomega.1c01693
ACS Omega 2021, 6, 14575−14584